



## Research article

Yongkang Gong, Kang Li\*, Nigel Copner, Heng Liu, Meng Zhao\*, Bo Zhang, Andreas Pusch, Diana L. Huffaker and Sang Soon Oh\*

# Integrated and spectrally selective thermal emitters enabled by layered metamaterials

<https://doi.org/10.1515/nanoph-2020-0578>

Received October 20, 2020; accepted December 5, 2020;  
published online January 5, 2021

**Abstract:** Nanophotonic engineering of light–matter interaction at subwavelength scale allows thermal radiation that is fundamentally different from that of traditional thermal emitters and provides exciting opportunities for various thermal-photonics applications. We propose a new kind of integrated and electrically controlled thermal emitter that exploits layered metamaterials with lithography-free and dielectric/metallic nanolayers. We demonstrate both theoretically and experimentally that the proposed concept can create a strong photonic bandgap in the visible regime and

allow small impedance mismatch at the infrared wavelengths, which gives rise to optical features of significantly enhanced emissivity at the broad infrared wavelengths of 1.4–14  $\mu\text{m}$  as well as effectively suppressed emissivity in the visible region. The electrically driven metamaterial devices are optically and thermally stable at temperatures up to  $\sim 800$  K with electro-optical conversion efficiency reaching  $\sim 30\%$ . We believe that the proposed high-efficiency thermal emitters will pave the way toward integrated infrared light source platforms for various thermal-photonics applications and particularly provide a novel alternative for cost-effective, compact, low glare, and energy-efficient infrared heating.

**Keywords:** infrared sources; nanophotonics; refractory metamaterials; thermal emitters.

**\*Corresponding authors: Kang Li**, Wireless and Optoelectronics Research and Innovation Centre, Faculty of Computing, Engineering and Science, University of South Wales, Cardiff, CF37 1DL, UK; and Foshan Huikang Optoelectronics Ltd., B Block, Sino-European Center, Foshan 528315, China, E-mail: kang.li@southwales.ac.uk; **Meng Zhao**, Jiangsu Key Laboratory of Micro and Nano Heat Fluid Flow Technology and Energy Application, School of Physical Science and Technology, Suzhou University of Science and Technology, Suzhou, 215009, China, E-mail: mzhao@usts.edu.cn; and **Sang Soon Oh**, School of Physics and Astronomy, Cardiff University, Cardiff, CF24 3AA, UK, E-mail: OhS2@cardiff.ac.uk

**Yongkang Gong and Diana L. Huffaker**, School of Physics and Astronomy, Cardiff University, Cardiff, CF24 3AA, UK, E-mail: gongy10@cardiff.ac.uk (Y. Gong), huffaker.diana@gmail.com (D.L. Huffaker). <https://orcid.org/0000-0002-2830-4423> (Y. Gong)

**Nigel Copner**, Foshan Huikang Optoelectronics Ltd., B Block, Sino-European Center, Foshan 528315, China; and Wireless and Optoelectronics Research and Innovation Centre, Faculty of Computing, Engineering and Science, University of South Wales, Cardiff, CF37 1DL, UK, E-mail: nigel.copner@southwales.ac.uk

**Heng Liu**, Jiangsu Key Laboratory of Micro and Nano Heat Fluid Flow Technology and Energy Application, School of Physical Science and Technology, Suzhou University of Science and Technology, Suzhou, 215009, China, E-mail: 1344846263@qq.com

**Bo Zhang**, Wireless and Optoelectronics Research and Innovation Centre, Faculty of Computing, Engineering and Science, University of South Wales, Cardiff, CF37 1DL, UK; and Henan Academy of Special Optics Ltd., Xinxiang, 453000, China

**Andreas Pusch**, School of Photovoltaic and Renewable Engineering, UNSW Sydney, Sydney, New South Wales 2052, Australia

## 1 Introduction

Artificial control of thermal radiation that is difficult to attain with natural materials has been a research topic of interest for decades. The principle of manipulating thermal radiation is based on Kirchhoff's law, which states that the emissivity of an object is equal to its absorptivity for a given frequency, polarization, and direction. In recent years, tremendous research efforts have been made toward tailoring light absorption based on plasmonic nanophotonics attributed to the recent unprecedented development of nanofabrication techniques. Metals are usually known to be perfect reflectors but when they are structured on a scale of the wavelength, light reflection fades away, and enhanced absorption occurs with a sharp spectrum much narrower than that of a blackbody due to excitation of resonant modes confined in the sub-wavelength metallic cavities or excitation of surface plasmon polaritons (SPPs) on the corrugated metal surfaces. Various types of spectrally selective narrowband nanophotonic absorbers have been developed such as nanogratings [1–4], photonic crystals [5–7], thin films [8], and three-layer-metamaterials [9–12]. These narrowband absorbers/emitters have triggered promising applications in

many different areas ranging from optical sensors [13–15], hot electron photodetectors [16], optical modulators [17–21], high-speed switching [22], energy recycling [23–25], and image encryption [26, 27] to thermal imaging [28].

In addition to the narrowband absorbers, recently there has been a strong motivation to enhance the light–matter interaction with a broadband absorption response by artificially manipulating the effective permittivity and permeability of nanophotonic structures to control the resonant modes. A number of strong broadband absorber schemes have been investigated, for example, by exploiting refractory metasurfaces [29–34], metal–insulator–metal nanostructures [35–38], semiconductor photonic crystals [39, 40], and multilayer thin films [41–45]. The broadband absorbers/emitters attract increased attention in fundamental science and have found a number of excited applications such as solar energy [46–48], thermophotovoltaics [32, 49, 50], infrared stealth [51], and radiative cooling [42, 43, 52].

In this paper, we propose and demonstrate a new kind of electrically controlled layered-metamaterial thermal emitters (LTEs) composed of multiple dielectric/metallic nanolayers. In contrast to the other reported nanophotonic thermal emitters, the proposed LTEs are thermal-photonic integrated and have advantage of tailoring thermal radiation with selectively enhanced emissivity in a broadband infrared regime and effectively suppressed emissivity at the visible wavelengths. We design and analyze the optical characteristics of the LTEs both analytically and numerically, and experimentally investigate their optical and thermal properties including angular-dependent emissivity, spectral radiation, thermal photonic properties, and electro-optical conversion efficiency. Our study offers a cost-effective, spectrally selective, and integrated infrared light source strategy that could find various applications. For example, it provides a solution that could possibly overcome the drawbacks of the existing infrared heater technologies (i.e., dazzling glare and low emissivity at the infrared wavelengths) [53].

## 2 Structure and design methodology

The proposed LTEs have a configuration featuring two stacked one-dimensional (1D) periodic lattices, as is illustrated in Figure 1A–C, where a finite periodic lattice (named as  $[\text{Si}/\text{Cr}/\text{Si}]^n$ ) with unit cell consisting of triple metallic/dielectric nanolayers of Si, Cr, and Si deposited on top of a  $\text{Ni}_{80}\text{Cr}_{20}$  thin film on a quartz substrate. On top of this lattice is another finite periodic lattice (denoted as

$[\text{SiO}_2/\text{Si}]^m$ ) with two alternately arranged nanolayers of  $\text{SiO}_2$  and Si. Here,  $m$  and  $n$  represent the number of the periods of the two lattices. The reason we choose  $\text{SiO}_2$  and Si materials for the top lattice is because of their high refractive index difference and high melting point. The former property enables broad photonic bandgap generation, while the latter allows the proposed LTEs to operate at the desired elevated temperature. The  $\text{SiO}_2$  layer is on top of the Si layer in the unit cell of the lattice  $(\text{SiO}_2/\text{Si})^m$ , thus constituting a cap layer  $\text{SiO}_2$  to protect the whole structure from oxidation. Electrical voltage is applied to the  $\text{Ni}_{80}\text{Cr}_{20}$  thin film to generate Joule heat to raise the temperature of the LTEs. We particularly choose  $\text{Ni}_{80}\text{Cr}_{20}$  as the electrically driven metallic layer, because  $\text{Ni}_{80}\text{Cr}_{20}$  material has high electrical resistivity and is efficient for generating Joule heat. The  $\text{Ni}_{80}\text{Cr}_{20}$  layer also acts as a light reflector and allows little transmitted light. Its thickness does not affect the optical properties of the LTEs in the considered wavelength range as long as it is thicker than hundreds of nanometers.

We model and design the proposed LTEs by starting with optimizing the top photonic lattice  $(\text{SiO}_2/\text{Si})^m$  to make the LTEs with low emissivity at the visible wavelengths. We investigate the optical spectra of the structure by the transfer matrix method (TMM) with the refractive indices of all materials taken from experimental data [54] and optimize the optical spectra by adjusting the nanolayers' thickness and the number of the periods of the lattice  $(\text{SiO}_2/\text{Si})^m$  (for detailed design and optimization, see Section A in Supplementary material). When the thickness of the thin film  $\text{SiO}_2$  (Si) is 100 nm (40 nm) and  $m$  is 4, broadband and high reflectivity at the wavelengths of 0.45–0.8  $\mu\text{m}$  is achieved in a broad angle of incidence (AOI) ranging from  $0^\circ$  up to  $80^\circ$  (see the inset of Figure 1D and Figure S2 in Supplementary material). According to the International Commission on Illumination (CIE) [55], there are three infrared radiation bands (i.e., IR-A 0.7–1.4  $\mu\text{m}$ , IR-B 1.4–3  $\mu\text{m}$ , and IR-C 3–1000  $\mu\text{m}$ ) and since the IR-B and IR-C bands are particularly important for many real-world applications such as chemical/medical sensing and infrared heating, we focus on designing the LTEs with enhanced emissivity at wavelengths of 1.4–14  $\mu\text{m}$ . To this end, we fix the geometric parameters of the optimized lattice  $(\text{SiO}_2/\text{Si})^m$  aforementioned, and then optimize the lattice  $(\text{Si}/\text{Cr}/\text{Si})^n$  to minimize the characteristic impedance difference  $|Z_{\text{LTEs}} - Z_{\text{air}}|$  to reduce reflectivity in the infrared regime and at the same time retain high reflectivity of the LTEs at the visible wavelengths, by adjusting the films' thicknesses and the number of lattice periods  $n$  (for the detailed optimization, see Equation S1 and Figure S3 in Supplementary

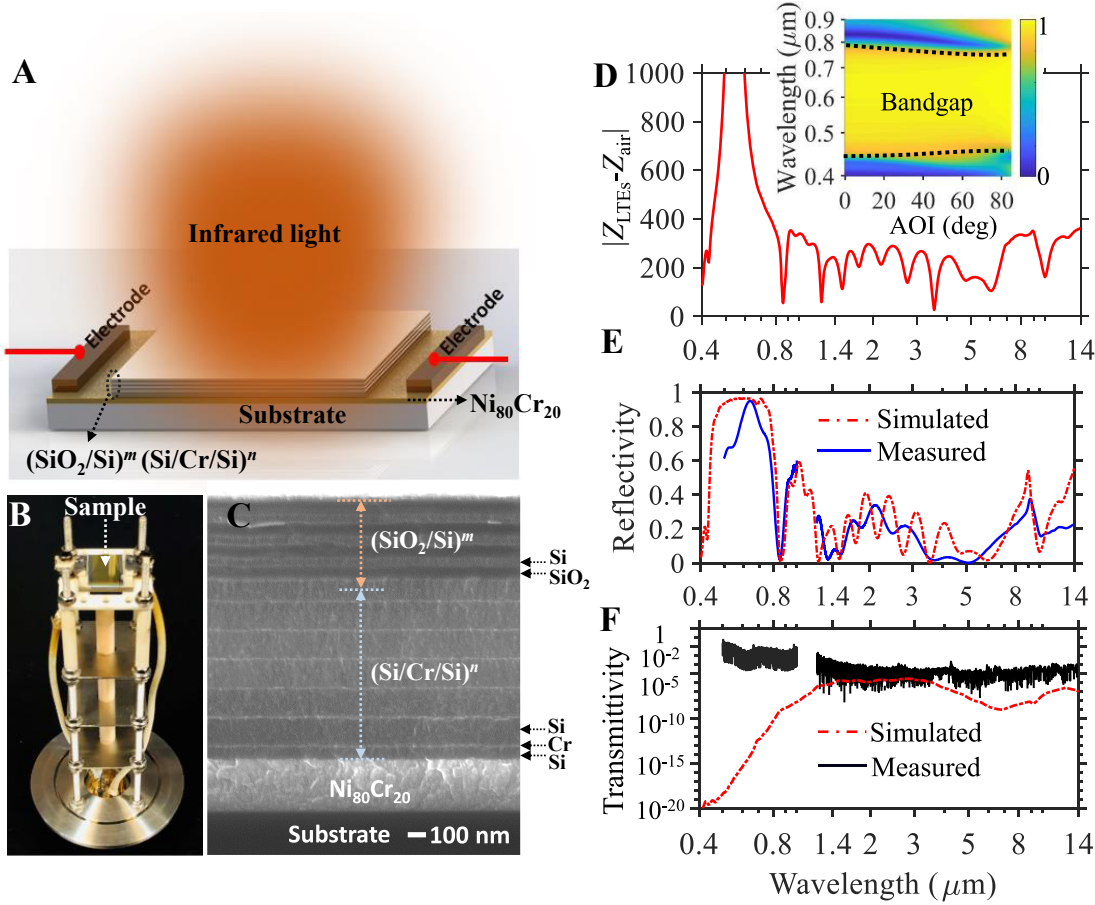


**Figure 1:** The concept, and the theoretical and experimental implementation of the selectively broadband metamaterial thermal emitters. (A) Schematic diagram of the LTEs, where two 1D photonic lattices with structures of  $(\text{Si}/\text{Cr}/\text{Si})^n$  and  $(\text{SiO}_2/\text{Si})^m$  are lying on top of a  $\text{Ni}_{80}\text{Cr}_{20}$  nanolayer deposited on a quartz substrate. Voltage is applied to the  $\text{Ni}_{80}\text{Cr}_{20}$  layer to generate Joule heat to raise the temperature of the whole device. Here,  $m$  and  $n$  represent the number of the periods of the two lattices. (B) Photography image of the fabricated devices mounted on a sample holder. (C) SEM image of the cross section of the LTEs. (D–F) The characteristic impedance mismatch  $|Z_{\text{LTEs}} - Z_{\text{air}}|$ , and the reflectivity and the transmissivity spectra, respectively. The inset of (D) depicts the reflectivity spectra versus angle of incidence (AOI) of the  $(\text{SiO}_2/\text{Si})^m$ . The geometric parameters of the LTEs are: the thickness of each Si ( $\text{SiO}_2$ ) layer in the  $(\text{SiO}_2/\text{Si})^m$  is 40 nm (100 nm), and the thickness of each Si (Cr) layer in the  $(\text{Si}/\text{Cr}/\text{Si})^n$  is 100 nm (4 nm); the number of periods  $m$  and  $n$  are 4 and 6, and the thickness of the  $\text{Ni}_{80}\text{Cr}_{20}$  layer and the substrate is 300 nm and 0.5 mm, respectively.

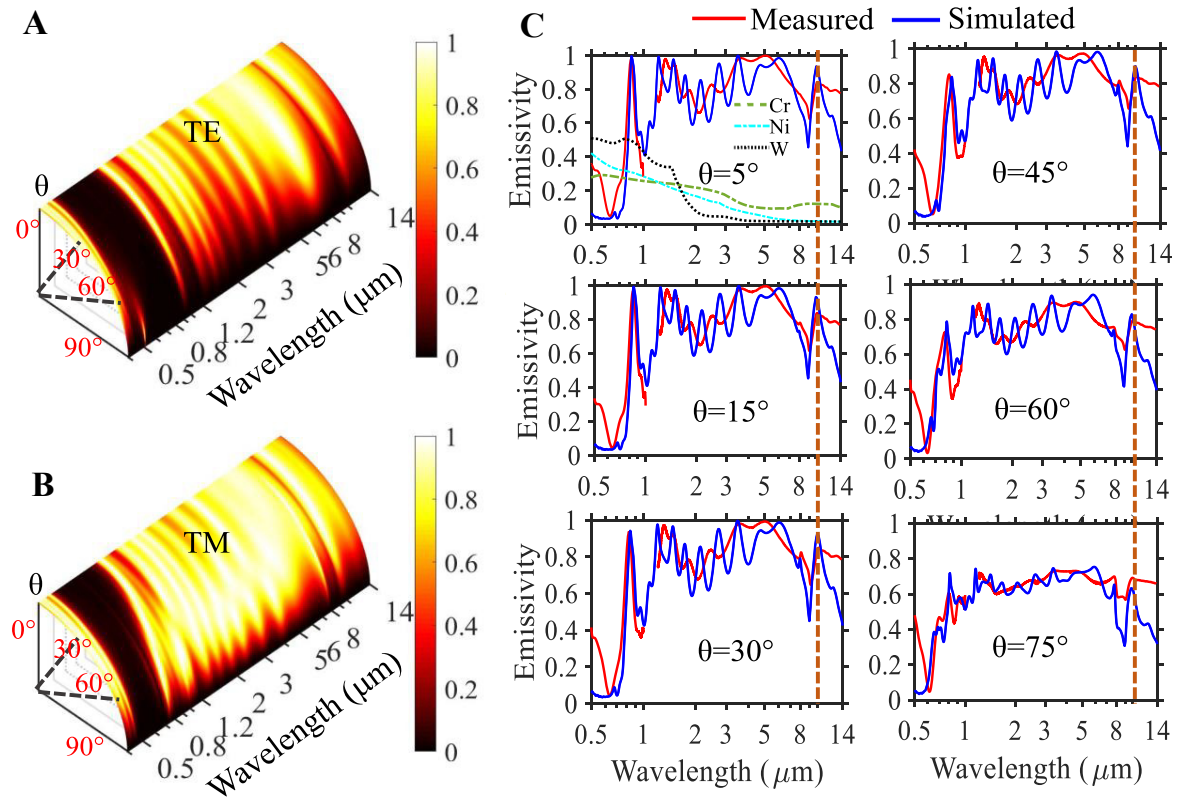
material). Here,  $Z_{\text{air}}$  and  $Z_{\text{LTEs}}$  are the characteristic impedance of air and the LTEs, respectively. The reflectivity of the LTEs is determined by  $R = |Z_{\text{LTEs}} - Z_{\text{air}}|^2 / |Z_{\text{LTEs}} + Z_{\text{air}}|^2$ , and a smaller impedance mismatch  $|Z_{\text{LTEs}} - Z_{\text{air}}|$  gives rise to a lower reflectivity. We observe from Figure 1D that the impedance mismatch at the visible wavelengths is large while the impedance mismatch at the infrared wavelengths is low when the thickness of Si (Cr) film is 100 nm (4 nm) and  $n$  is 6. Therefore, the light reflection at the visible wavelengths dominates the infrared light reflection for this configuration. This is verified by the reflectivity spectra numerically calculated by TMM, as depicted in Figure 1E, where high reflectivity at the wavelengths of 0.45–0.75  $\mu\text{m}$  and low reflectivity at the wavelengths of 1.4–14  $\mu\text{m}$  is achieved.

This selectively ultrabroadband reflectivity characteristic enables LTEs with high absorptivity in the infrared regime and low absorptivity in the visible regime, considering the transmissivity of the proposed LTEs is tiny at all the considered wavelengths (Figure 1F). Photonic lattices with unit cells consisting of dual metallic/dielectric nanolayers were reported to allow broadband emissivity features [44, 56]. In the proposed configuration, the lattice with triple nanolayers per unit cell enables larger emissivity than the lattices with dual nanolayer unit cells at the infrared wavelengths (see Figure S4 in Supplementary material). Lattices with unit cells having more nanolayers could further increase the emissivity, but it may degrade the thermomechanical performance of the proposed LTEs.

### 3 Device fabrication and optical spectra measurements

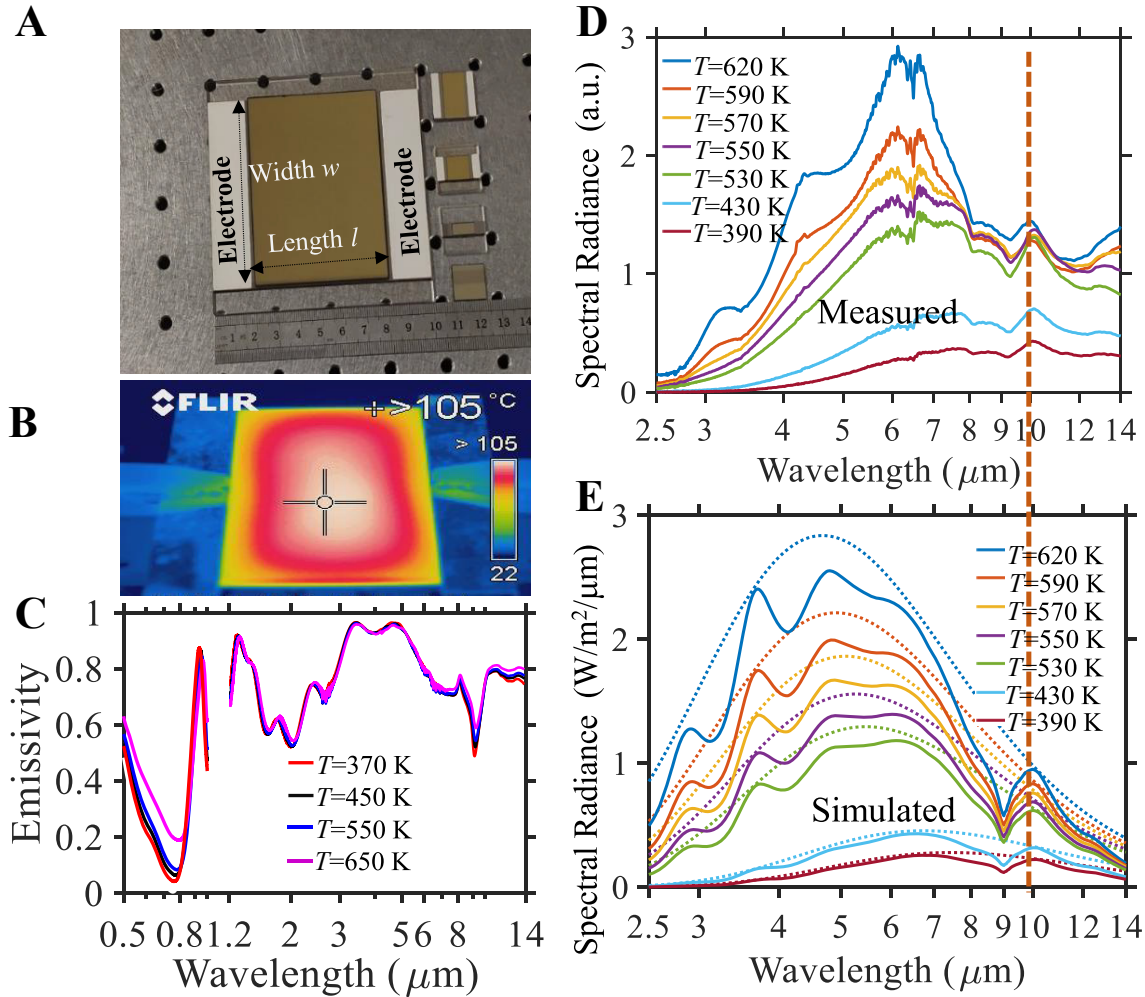
We fabricate the designed LTEs using E-beam evaporation and measure angle-dependent reflectivity and transmissivity spectra by Fourier-transform infrared spectroscopy (FTIR) and grating spectrometer (for fabrication and measurement details, see Sections B and C in Supplementary material). The measured reflectivity and transmissivity spectra are consistent with the theoretical prediction, as demonstrated in Figure 1E and F. Based on the reflectivity and transmissivity, we obtain the spectral hemispherical absorptivity  $A(\theta, \lambda)$  of the LTEs for both transverse-electric (TE)- and transverse-magnetic (TM)-polarized light, where  $\theta$  and  $\lambda$  is AOI and wavelength, respectively. The absorptivity has no azimuthal angle dependence and only has polar angle dependence due to the one-dimensional geometry of the LTEs. It is noted from

Figure 2A and B that both TE- and TM-polarized light experience high (low) absorptivity in a broad spectral and angular range at the infrared (visible) wavelengths. The angle-dependent emissivity of the LTEs is derived by averaging the TE- and TM-polarized absorptivity. The simulated and measured emissivity spectra at various angles from  $5^\circ$  to  $75^\circ$  are plotted and compared in Figure 2C, showing a good agreement between our theory and experiment. Figure 2C indicates that in comparison with the typical thermal emitter metals (such as Ni, Cr, and W) that suffer from high (low) emissivity in the visible (infrared) regime, the proposed LTEs have the advantage of suppressed emissivity at visible wavelengths and enhanced emissivity at the infrared wavelengths with a broad spectral and angular response. At the angle of  $\theta = 5^\circ$ , for example, the calculated emissivity is as high as  $\sim 0.81$  averaged over wavelengths of  $1.4\text{--}14\ \mu\text{m}$ , and is as low as  $\sim 0.07$  averaged over wavelengths of  $0.45\text{--}0.75\ \mu\text{m}$ . Emissivity peaks at a wavelength of  $\sim 10\ \mu\text{m}$  is noticed at all the angles, as indicated by the vertical lines in



**Figure 2:** The spectral characteristics of the LTEs at different angle and polarization.

(A), (B) The calculated absorptivity spectra versus the angle of incidence for the TE- and TM-polarized light, respectively. (C) The measured and calculated emissivity spectra at various angles from  $5^\circ$  to  $75^\circ$ . The calculated emissivity is obtained by averaging the TE- and TM-polarized absorptivity spectra from (A), while the measured emissivity is derived from collecting variable angle specular reflectance with unpolarized light illumination. The emissivity spectra of the LTEs are compared with that of a 300 nm-thick thin films of refractory metals (tungsten [W], nickel [Ni], and chromium [Cr]) that are widely used for thermal emitters, demonstrating that the proposed structures offer enhanced (suppressed) emissivity in the infrared (visible) regime. The vertical lines in (C) indicate the presence of an emissivity peak at  $\sim 10\ \mu\text{m}$ . The structure geometric parameters are the same as in Figure 1.



**Figure 3:** The optical emissivity and thermal radiation of the LTEs at elevated temperature.

(A) A photograph of the fabricated LTEs with different width  $w$  and length  $l$ . (B) The thermal distribution of the samples taken by an infrared camera. (C) The measured emissivity at the angle of  $\theta = 45^\circ$  under different structure temperature obtained by controlling the voltage applied to the  $\text{Ni}_{80}\text{Cr}_{20}$  layer. (D) The measured spectral radiation intensity versus the device temperature by directing the radiated light into a parabolic mirror to be collimated into a FTIR for detection. (E) The calculated spectra radiance (solid lines) compared to that of an ideal blackbody (dotted lines) at the same operating temperature. The calculations are performed by integrating the emitted light within divergence angle of  $5^\circ$  from the normal of the LTEs (see Equation S2 in Supplementary material). Both the measured and calculated spectra show a peak at  $\sim 10 \mu\text{m}$  (marked by the vertical dashed line) due to strong emissivity at this wavelength (see the vertical dashed line in Figure 2C). The structure geometries are the same as those in Figure 2.

Figure 2C. This is due to high light absorption induced by the large imaginary part of the refractive index of the  $\text{SiO}_2$  thin films at this wavelength.

## 4 Emissivity and thermal radiation at high temperature

An important question is whether the thermal emitters are optically and thermally stable at high temperatures. To this end, we fabricate LTEs with different structure dimension

of width  $w$  and length  $l$  (see Figure 3A) and undertake a series of high temperature measurements. We measure the spectral emissivity and thermal radiation of the LTEs at different operating temperatures controlled by the electric current flowing through the  $\text{Ni}_{80}\text{Cr}_{20}$  thin film (for detailed experimental measurements, see Section C in Supplementary material). The generated Joule heat depends on both the input electrical voltage and the structure resistance that relies on the size of the  $\text{Ni}_{80}\text{Cr}_{20}$  film. We measure the  $I$ - $V$  curve of the fabricated LTEs with different structure size and show that the structure resistance decreases with  $w$  and increases with  $l$  (see

Figure S4 in Supplementary material). The thermal image of the electrically heated LTEs taken by an infrared camera (Figure 3B) shows uniform temperature distribution on the surface with slightly decreased temperature at the edges due to thermal convection from the structure to the ambient environment. We evaluate the optical stability of the LTEs by measuring the emissivity spectra at different operating temperatures. Figure 3C clearly demonstrates that the emissivity does not degrade much at high temperatures especially at the infrared wavelengths, although a slight increase of the emissivity is observed at the visible wavelengths due to the expected increase of the electron collision frequency at high temperatures, which leads to increased free carrier absorption.

To investigate the thermal radiation property, we collimate and direct the radiated light of LTEs into a FTIR to measure the radiated power as function of the operating temperature of the LTEs (for the detailed experimental setup, see Sections C and D in Supplementary material). Figure 3D illustrates that the thermal radiation becomes stronger when the device temperature increases, which is consistent with simulated results in Figure 3E. A spectral peak at  $\sim 10 \mu\text{m}$  is observed in both measurements and simulations, as marked by the vertical dashed line in Figure 3D and E, which is due to the high emissivity peak around this wavelength (see the vertical dashed lines in Figure 2C). The discrepancies between the measurements and simulations are caused by several factors. For example, the surface temperature of the LTEs is not perfectly uniform as assumed in simulations, and it is impossible to well collimate the radiated light at all the wavelengths to the detector for measurements since the LTEs radiate light covering broad wavelengths. We also compare the thermal radiation of LTEs with an ideal blackbody and show that the proposed LTEs give rise to radiation spectra that are very close to that of the blackbody at the same operating temperature (Figure 3E).

## 5 Properties of the thermal photonic dynamics

To fully characterize the thermal photonic performance of LTEs, it is essential to explore how it responds to the input electricity in real time. To do this, we gradually increase the voltage applied to the  $\text{Ni}_{80}\text{Cr}_{20}$  layer with ramp rate of 0.1 V per 15 min (see the inset of Figure 4A) to

ensure there is enough time for the temperature to increase and get stabilized. At the same time, we monitor the evolution of the current, the surface temperature, and the radiated power. We place the electrically controlled LTEs in a vacuum chamber and put it very close to the KBr window of the chamber (for the detailed measurement system, see Section E and Figure S6 in Supplementary material). The radiation from the heated LTEs passes through the KBr window and enters the input port of a gold-coated integrating sphere that sits very closely to the other side of the KBr window, and a photodetector is placed at the exit port of the integrating sphere to collect the light and measure the power. We see from Figure 4A that the current, the device surface temperature, and the radiated power (measured at the exit port of the integrating sphere) increases with the applied voltage until the temperature reaches  $\sim 800$  K. When the voltage is further increased, the nanolayers of the LTEs crack and the LTEs are not conductive any longer. As a result, the current, the temperature, and the radiated power drop dramatically. We calibrate the integrating sphere with a commercial blackbody and measure the blackbody radiation power  $P_1$  at the input port of the integrating sphere and the light power  $P_2$  at the exit port of the integrating sphere, and derive the transmission efficiency of the integrating sphere by  $\eta = P_2/P_1 = \sim 0.065\%$  (see Figure S8 in Supplementary material). By normalizing the light power in Figure 4A to  $\eta$ , we get the power  $P_o$  of the light radiated from the LTEs. The evolution of  $P_o$  and the surface temperature to the input electricity power  $P_e$  is given in Figure 4B. Based on the results, we obtain the electro-optical conversion efficiency of the LTEs by extracting  $P_o$  versus  $P_e$ . Figure 4C shows that the conversion efficiency reaches  $\sim 30\%$  at temperature  $> 700$  K. The conversion efficiency can be further increased by means of, for example, minimizing the thermal contact between the sample and the sample holder to reduce thermal conduction and increasing the chamber vacuum to reduce thermal convection (see Equations S3–S5 in Supplementary material).

## 6 Conclusions

We have proposed an integrated thermophotonic layered metamaterial scheme to obtain efficient and spectrally selective thermal emitters with greatly enhanced emissivity in the infrared regime and effectively suppressed emissivity in the visible regime. With our optimized thermal emitters, we have achieved an averaged emissivity as

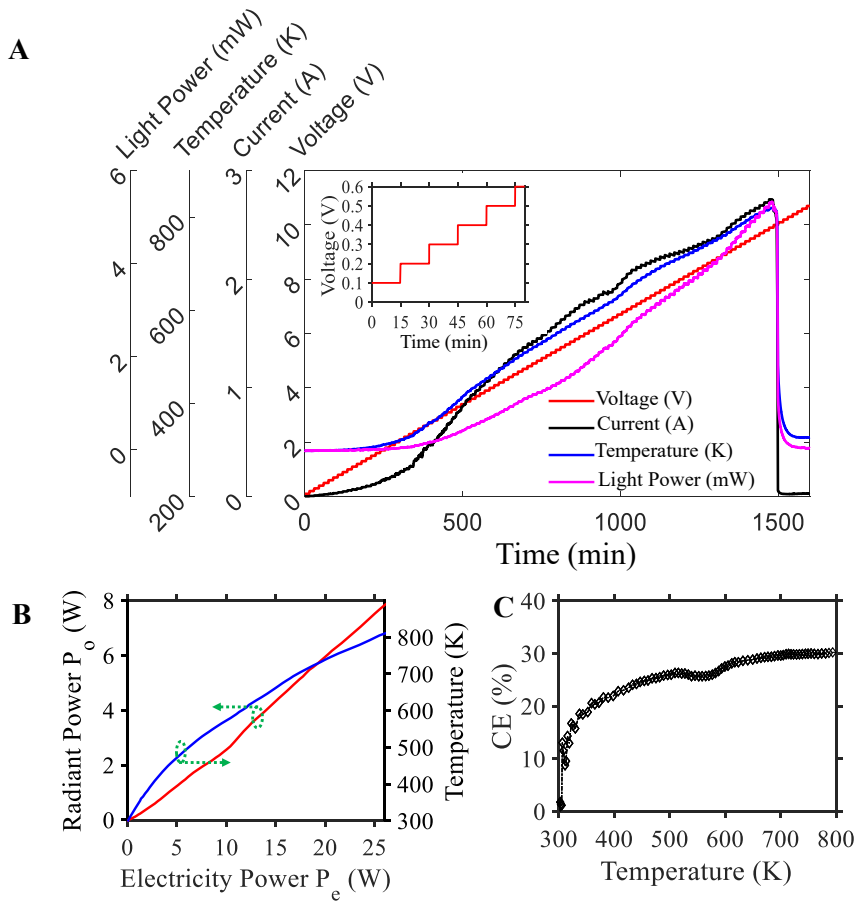


**Figure 4:** The thermal photonic dynamics of the electrically controlled LTEs.

(A) The evolution of the current, the surface temperature, and the radiated power (detected at the exit port of the integrating sphere) to the input electrical voltage that increases with a step of 0.1 V per 15 min. The inset plots the zoom-in of the voltage versus time. The light radiated from the LTEs propagates through the KBr window of the vacuum chamber and enters the integrating sphere through the input port, and then is detected by a photodetector at the exit port of the integrating sphere. (B) The dependence of the radiant light power  $P_o$  (at the input port of the integrating sphere) on the input electrical power  $P_e$  and the surface temperature of the LTEs. (C) The electro-optical conversion efficiency  $CE = P_o/P_e$  of the LTEs. The thickness of the structure nanolayers are the same as those in Figure 3, and the structure width is  $w = 20$  mm and length is  $l = 10$  mm.

high as  $\sim 0.81$  over an broad infrared wavelength range of  $1.4\text{--}14\ \mu\text{m}$  and an averaged emissivity as low as  $\sim 0.07$  at visible wavelengths of  $0.45\text{--}0.75\ \mu\text{m}$ . We have experimentally verified the proposed concept by exploring the optical and thermal characteristics including the angular- and temperature-dependent emissivity, the spectral radiation, the thermal dynamics, and the electro-optical conversion efficiency. Our measurement results demonstrate that proposed LTE devices are optically and thermally stable up to  $\sim 800$  K and yield an electro-optical conversion of  $\sim 30\%$ . Another advantage of the LTEs is the feature of one-dimensional structural simplicity, which allows large-scale production with low-cost fabrication. We believe the LTEs offer an enhanced and integrated infrared source strategy that could find promising applications such as infrared heating, thermophotovoltaics, and thermal imaging etc. Finally, we stress that the thermal photonic performance of the LTEs could be further improved of by incorporating the proposed concept with other dielectric and metal materials (such as tungsten, hafnium dioxide, and aluminum oxide) that have better thermal and mechanical stability.

**Acknowledgments:** The authors gratefully acknowledge Zhibo Li and Shiyu Xie for their assistance in the device characterization and valuable discussions. We thank Rui Dong and Dominic Kwan for the help with the FTIR measurements.

**Author contributions:** Y.G. conceived the project. Y.G., K.L., and N.C. performed designs and numerical simulations. K.L. and B.Z. implemented device fabrications. Y.G. and K.L. set up the system for the emissivity and reflectivity spectra measurement. M.Z. and H.L. built the high-temperature characterization setup and undertook characterization of the device thermal photonic radiation. Y.G. wrote the manuscript with major contributions from S.S.O. and A.P. All authors discussed the simulated and measured results and the manuscript. All authors have given approval to submission of the manuscript.

**Research funding:** This work was supported by 2015 Foshan Technology Innovation Group project (Advanced Solid-State Light Source Application and Innovation Team) and European Regional Development Fund through the Welsh Government (80762-CU145 (East)).

**Conflict of interest statement:** The authors declare no conflicts of interest regarding this article.

## References

- [1] K. Ikeda, H. T. Miyazaki, T. Kasaya, et al., “Controlled thermal emission of polarized infrared waves from arrayed plasmon nanocavities,” *Appl. Phys. Lett.*, vol. 92, p. 021117, 2008.
- [2] Y. Qu, Q. Li, H. Gong, et al., “Spatially and spectrally resolved narrowband optical absorber based on 2D grating nanostructures on metallic films,” *Adv. Opt. Mater.*, vol. 4, pp. 480–486, 2016.
- [3] N. Bonod, G. Tayeb, D. Maystre, S. Enoch, and E. Popov, “Total absorption of light by lamellar metallic gratings,” *Opt. Express*, vol. 16, pp. 15431–15438, 2008.
- [4] H. Sai, Y. Kanamori, and H. Yugami, “High-temperature resistive surface grating for spectral control of thermal radiation,” *Appl. Phys. Lett.*, vol. 82, pp. 1685–1687, 2003.
- [5] S. Y. Lin, J. Moreno, and J. G. Fleming, “Three-dimensional photonic-crystal emitter for thermal photovoltaic power generation,” *Appl. Phys. Lett.*, vol. 83, pp. 380–382, 2003.
- [6] V. Rinnerbauer, A. Lenert, D. M. Bierman, et al., “Metallic photonic crystal absorber-emitter for efficient spectral control in high-temperature solar thermophotovoltaics,” *Adv. Energy Mater.*, vol. 4, p. 1400334, 2014.
- [7] J. G. Fleming, S. Y. Lin, I. El-Kady, R. Biswas, and K. M. Ho, “All-metallic three-dimensional photonic crystals with a large infrared bandgap,” *Nature*, vol. 417, pp. 52–55, 2002.
- [8] X. Liu, Z. Li, Z. Wen, et al., “Large-area, lithography-free, narrowband and highly directional thermal emitter,” *Nanoscale*, vol. 11, pp. 19742–19750, 2019.
- [9] N. I. Landy, S. Sajuyigbe, J. J. Mock, D. R. Smith, and W. J. Padilla, “Perfect metamaterial absorber,” *Phys. Rev. Lett.*, vol. 100, p. 207402, 2008.
- [10] X. L. Liu, T. Tyler, T. Starr, et al., “Taming the blackbody with infrared metamaterials as selective thermal emitters,” *Phys. Rev. Lett.*, vol. 107, p. 045901, 2011.
- [11] Y. Cui, Y. He, Y. Jin, et al., “Plasmonic and metamaterial structures as electromagnetic absorbers,” *Laser Photonics Rev.*, vol. 8, pp. 495–520, 2014.
- [12] D. Shrekenhamer, W.-C. Chen, and W. J. Padilla, “Liquid crystal tunable metamaterial absorber,” *Phys. Rev. Lett.*, vol. 110, p. 177403, 2013.
- [13] N. Liu, M. Mesch, T. Weiss, M. Hentschel, and H. Giessen, “Infrared perfect absorber and its application as plasmonic sensor,” *Nano Lett.*, vol. 10, pp. 2342–2348, 2010.
- [14] A. Tittl, P. Mai, R. Taubert, et al., “Palladium-based plasmonic perfect absorber in the visible wavelength range and its application to hydrogen sensing,” *Nano Lett.*, vol. 11, pp. 4366–4369, 2011.
- [15] A. Lochbaum, Y. Fedoryshyn, A. Dorodnyy, et al., “On-Chip narrowband thermal emitter for mid-IR optical gas sensing,” *ACS Photonics*, vol. 4, pp. 1371–1380, 2017.
- [16] W. Li and J. Valentine, “Metamaterial perfect absorber based hot electron photodetection,” *Nano Lett.*, vol. 14, pp. 3510–3514, 2014.
- [17] V. W. Brar, M. C. Sherrott, M. S. Jang, et al., “Electronic modulation of infrared radiation in graphene plasmonic resonators,” *Nat. Commun.*, vol. 6, p. 7032, 2015.
- [18] Y. Miyoshi, Y. Fukazawa, Y. Amasaka, et al., “High-speed and on-chip graphene blackbody emitters for optical communications by remote heat transfer,” *Nat. Commun.*, vol. 9, p. 1279, 2018.
- [19] Y. Yao, R. Shankar, M. A. Kats, et al., “Electrically tunable metasurface perfect absorbers for ultrathin mid-infrared optical modulators,” *Nano Lett.*, vol. 14, pp. 6526–6532, 2014.
- [20] E. Sakat, L. Wojszwyk, J. P. Hugonin, et al., “Enhancing thermal radiation with nanoantennas to create infrared sources with high modulation rates,” *Optica*, vol. 5, pp. 175–179, 2018.
- [21] Z. H. Zhu, P. G. Evans, R. F. Haglund, and J. G. Valentine, “Dynamically reconfigurable metadvice employing nanostructured phase-change materials,” *Nano Lett.*, vol. 17, pp. 4881–4885, 2017.
- [22] T. Inoue, M. De Zoysa, T. Asano, and S. Noda, “On-chip integration and high-speed switching of multi-wavelength narrowband thermal emitters,” *Appl. Phys. Lett.*, vol. 108, p. 091101, 2016.
- [23] W. Li and S. H. Fan, “Nanophotonic control of thermal radiation for energy applications [Invited],” *Opt. Express*, vol. 26, pp. 15995–16021, 2018.
- [24] D. N. Woolf, E. A. Kadlec, D. Bethke, et al., “High-efficiency thermophotovoltaic energy conversion enabled by a metamaterial selective emitter,” *Optica*, vol. 5, pp. 213–218, 2018.
- [25] M. De Zoysa, T. Asano, K. Mochizuki, et al., “Conversion of broadband to narrowband thermal emission through energy recycling,” *Nat. Photonics*, vol. 6, pp. 535–539, 2012.
- [26] M. Makhsiyani, P. Bouchon, J. Jaeck, J. L. Pelouard, and R. Haider, “Shaping the spatial and spectral emissivity at the diffraction limit,” *Appl. Phys. Lett.*, vol. 107, p. 251103, 2015.
- [27] G. Bakan, S. Ayas, M. Serhatlioglu, C. Elbuken, and A. Dana, “Invisible thin-film patterns with strong infrared emission as an optical security feature,” *Adv. Opt. Mater.*, vol. 6, p. 1800613, 2018.
- [28] A. Tittl, A. K. U. Michel, M. Schaferling, et al., “A switchable mid-infrared plasmonic perfect absorber with multispectral thermal imaging capability,” *Adv. Mater.*, vol. 27, pp. 4597–4603, 2015.
- [29] W. Li, U. Guler, N. Kinsey, et al., “Refractory plasmonics with titanium nitride: broadband metamaterial absorber,” *Adv. Mater.*, vol. 26, pp. 7959–7965, 2014.
- [30] P. Yu, L. V. Besteiro, Y. J. Huang, et al., “Broadband metamaterial absorbers,” *Adv. Opt. Mater.*, vol. 7, p. 1800995, 2019.
- [31] T. Yokoyama, T. D. Dao, K. Chen, et al., “Spectrally selective mid-infrared thermal emission from molybdenum plasmonic metamaterial operated up to 1000 °C,” *Adv. Opt. Mater.*, vol. 4, pp. 1987–1992, 2016.
- [32] C. C. Chang, W. J. M. Kort-Kamp, J. Nogan, et al., “High-temperature refractory metasurfaces for solar thermophotovoltaic energy harvesting,” *Nano Lett.*, vol. 18, pp. 7665–7673, 2018.
- [33] Y. K. Li, W. Li, Y. Wang, J. Cao, and J. G. Guan, “Refractory metamaterial microwave absorber with strong absorption insensitive to temperature,” *Adv. Opt. Mater.*, vol. 6, p. 1800691, 2018.
- [34] Y. X. Yeng, M. Ghebrehan, P. Bermel, et al., “Enabling high-temperature nanophotonics for energy applications,” *Proc. Natl. Acad. Sci.*, vol. 109, pp. 2280–2285, 2012.
- [35] K. Aydin, V. E. Ferry, R. M. Briggs, and H. A. Atwater, “Broadband polarization-independent resonant light absorption using ultrathin plasmonic super absorbers,” *Nat. Commun.*, vol. 2, p. 517, 2011.

- [36] Y. K. Gong, Z. B. Wang, K. Li, et al., “Highly efficient and broadband mid-infrared metamaterial thermal emitter for optical gas sensing,” *Opt. Lett.*, vol. 42, pp. 4537–4540, 2017.
- [37] M. Aalizadeh, A. Khavasi, B. Butun, and E. Ozbay, “Large-Area, cost-effective, ultra-broadband perfect absorber utilizing manganese in metal-insulator–metal structure,” *Sci. Rep.*, vol. 8, p. 9162, 2018.
- [38] J. Hao, J. Wang, X. Liu, et al., “High performance optical absorber based on a plasmonic metamaterial,” *Appl. Phys. Lett.*, vol. 96, p. 251104, 2010.
- [39] S. Shrestha, Y. Wang, A. C. Overvig, et al., “Indium tin oxide broadband metasurface absorber,” *ACS Photonics*, vol. 5, pp. 3526–3533, 2018.
- [40] T. Asano, M. Suemitsu, K. Hashimoto, et al., “Near-infrared-to-visible highly selective thermal emitters based on an intrinsic semiconductor,” *Sci. Adv.*, vol. 2, p. e1600499, 2016.
- [41] C. Y. Yang, C. G. Ji, W. D. Shen, et al., “Compact multilayer film structures for ultrabroadband, omnidirectional, and efficient absorption,” *ACS Photonics*, vol. 3, pp. 590–596, 2016.
- [42] Y. Zhai, Y. G. Ma, S. N. David, et al., “Scalable-manufactured randomized glass-polymer hybrid metamaterial for daytime radiative cooling,” *Science*, vol. 355, pp. 1062–1066, 2017.
- [43] A. P. Raman, M. A. Anoma, L. Zhu, E. Rephaeli, and S. Fan, “Passive radiative cooling below ambient air temperature under direct sunlight,” *Nature*, vol. 515, pp. 540–544, 2014.
- [44] A. Ghobadi, H. Hajian, B. Butun, and E. Ozbay, “Strong light–matter interaction in lithography-free planar metamaterial perfect absorbers,” *ACS Photonics*, vol. 5, pp. 4203–4221, 2018.
- [45] K.-K. Du, Q. Li, Y.-B. Lyu, et al., “Control over emissivity of zero-static-power thermal emitters based on phase-changing material GST,” *Light Sci. Appl.*, vol. 6, p. e16194, 2017.
- [46] L. Zhou, Y. L. Tan, D. X. Ji, et al., “Self-assembly of highly efficient, broadband plasmonic absorbers for solar steam generation,” *Sci. Adv.*, vol. 2, p. e1501227, 2016.
- [47] Y. Wang, L. Zhou, Y. Zhang, et al., “Hybrid solar absorber-emitter by coherence-enhanced absorption for improved solar thermophotovoltaic conversion,” *Adv. Opt. Mater.*, vol. 6, p. 1800813, 2018.
- [48] W. Wang, S. Wu, K. Reinhardt, Y. Lu, and S. Chen, “Broadband light absorption enhancement in thin-film silicon solar cells,” *Nano Lett.*, vol. 10, pp. 2012–2018, 2010.
- [49] A. Lenert, D. M. Bierman, Y. Nam, et al., “A nanophotonic solar thermophotovoltaic device,” *Nat. Nanotechnol.*, vol. 9, pp. 126–130, 2014.
- [50] D. M. Bierman, A. Lenert, W. R. Chan, et al., “Enhanced photovoltaic energy conversion using thermally based spectral shaping,” *Nat. Energy*, vol. 1, p. 16068, 2016.
- [51] L. Peng, D. Q. Liu, H. F. Cheng, S. Zhou, and M. Zu, “A multilayer film based selective thermal emitter for infrared stealth Technology,” *Adv. Opt. Mater.*, vol. 6, p. 1801006, 2018.
- [52] L. Fan, W. Li, W. Jin, M. Orenstein, and S. Fan, “Maximal nighttime electrical power generation via optimal radiative cooling,” *Opt. Express*, vol. 28, pp. 25460–25470, 2020.
- [53] Space heating is a huge source of energy consumption. In comparison with the air space heating technologies (i.e., heat is generated by electricity/gas and dissipates into air) that is very inefficient since Heat Conveys to the Whole Space, Infrared Heating Provides Optical Heating Locally and Instantly and Has Reported to Be More Energy Efficient. The Existing Commercial Infrared Panels (Typically Made of Refractory Metals Such as Tungsten, Nichrome Alloys, and Ceramic Materials Etc), However, Have Two Major Issues that Have Inhibited the Market Penetration to Industry and Homeowners: Dazzling Glare and Low Efficiency. The Glare Occurs Due to Strong Radiation in Visible Wavelengths, Which Not Only Causes Light Pollution. The Low Efficiency Arises from Low Optical Emissivity of the Infrared Panels at the Infrared Wavelengths. Enhancing Infrared Heating Performance Relies on Material Innovation of Increasing Emissivity in Infrared Regime and Decreasing Emissivity at Visible Wavelengths
- [54] E. D. Palik, *Handbook of Optical Constants of Solids*, London, Academic Press, 1998.
- [55] International Commission on Non-Ionizing Radiation Protection, “ICNIRP guidelines on limits of exposure to incoherent visible and infrared radiation,” *Health Phys.*, vol. 105, pp. 74–96, 2013.
- [56] P. N. Dyachenko, S. Molesky, A. Y. Petrov, et al., “Controlling thermal emission with refractory epsilon-near-zero metamaterials via topological transitions,” *Nat. Commun.*, vol. 7, p. 11809, 2016.

---

**Supplementary Material:** Supplementary material is available and includes design strategy and device optimization, fabrication of the designed LTEs, angular dependent reflection measurements, spectral thermal radiation, characterization of thermal photonic dynamics and the total radiated power and electro-optical conversion efficiency.

The online version of this article offers supplementary material (<https://doi.org/10.1515/nanoph-2020-0578>).